MedChemComm

CONCISE ARTICLE

View Article Online
View Journal

Cite this: DOI: 10.1039/c5md00247h

Navigating into the chemical space between MGCD0103 and SAHA: novel histone deacetylase inhibitors as a promising lead†‡

Xin Zhang,§[ab] Peng-Cheng Lv,§[ab] Dong-Dong Li,[ab] Wei-Ming Zhang*[ab] and Hai-Liang Zhu*[ab]

Received 10th June 2015,
Accepted 13th August 2015

DOI: 10.1039/c5md00247h

www.rsc.org/medchemcomm

Histone deacetylase inhibitors (HDIs) are an increasingly important class of cancer-targeting agents. Two kinds of small molecule histone deacetylase inhibitors, mainly employing the motifs of the two known HDAC inhibitors MGCD0103 and SAHA as the basic scaffolds, were designed, synthesized and evaluated for the preliminary biological activity. Strikingly, these two compounds regained a long half-life potency like MGCD0103 and retained the non-selectivity for HDAC1 *versus* HDAC6 derived from SAHA. Together, these two compounds combining both the advantages of MGCD0103 and SAHA could be considered as novel histone deacetylase inhibitors in targeted drug development and possibly anticipated to be more effective under the clinical trials.

Introduction

Histone deacetylases (HDACs) have been proven to be one of the most promising targets in cancer drug development over the past few years.[1] They accurately control the process of lysine acetylation and deacetylation in the epigenetic field, together with histone acetyltransferases (HATs), finally leading to gene transcription or silencing.[2] In addition, there are 18 members that are divided into four classes in the human HDAC family, and about 50 nonhistone proteins have been discovered as HDAC substrates.[2] Therefore, the biological interaction map in the centre of HDAC seems to be complicated. While HDAC proteins, particularly class I and II members, are more linked to carcinogenesis, the detailed molecular mechanism connecting HDAC activity to cancer has not yet been defined, and the precise function of each isoform in cancer cell remains unclear.[3] However, the recent development of HDAC inhibitors (HDIs) can contribute to the success of cancer therapy, particularly adopting the strategy in combination with other antitumor agents in the clinical trial.[4]

So far, at least 16 kinds of HDAC inhibitors are being evaluated under the clinical stage (Fig. 5). Among them, the two drugs vorinostat (SAHA, an unselective HDAC inhibitor) and romidepsin (FK-228) have been approved by the US Food and Drug Administration for cutaneous T-cell lymphoma in 2006 and 2009, respectively.[5,6] Although it remains unclear whether selective HDAC inhibitors would provide advantages at the utility and potential therapeutic level when compared to the pan-inhibitor SAHA widely used in clinical trials, selective inhibitors can clearly aid in exploring the molecular mechanism connecting HDAC activity to cancer formation, which might provide a more effective chemotherapy.[3] As expected, the emerging trends in the development of HDAC inhibitors have focused on the class-selective or isoform-selective aspect (Fig. 1), based on the analysis of a recently published paper on HDAC inhibitors primarily abstracted from the *Journal of Medicinal Chemistry*.

One of highlights in this paper is using fragment-based drug design (FBDD), which has emerged as a powerful strategy in lead discovery.[7,8] The basis of this approach generally involves screening a relatively small library of fragments. All fragments used in this paper are cut from clinical drugs and have been proven to be the most optimal. Therefore, the current process of screening has included a lot of SAR discussions before and our design leads to further optimization of activity and selectivity. According to the canonical framework, most of the HDIs could be decomposed into one capping group that interacts with the residues at the entrance of the active site, one linker that lies into the hydrophobic space of the binding site tunnel, and one Zn-binding group (ZBG) able to chelate with the Zn^{2+} at the bottom of the cavity (Fig. 1).

[a] *Nanjing Institute for the Comprehensive Utilization of Wild Plant, Nanjing 210042, People's Republic of China. E-mail: zhuhl@nju.edu.cn; Fax: +86 25 8359 2672; Tel: +86 25 8359 2572*

[b] *State Key Laboratory of Pharmaceutical Biotechnology, Nanjing University, Nanjing 210093, People's Republic of China*

† Electronic supplementary information (ESI) available: Chemistry details for the syntheses of two target compounds and figures for ^{1}H NMR, ESI and antiproliferative assay. See DOI: 10.1039/c5md00247h

‡ The authors declare no competing financial interest.

§ These two authors equally contributed to this paper.

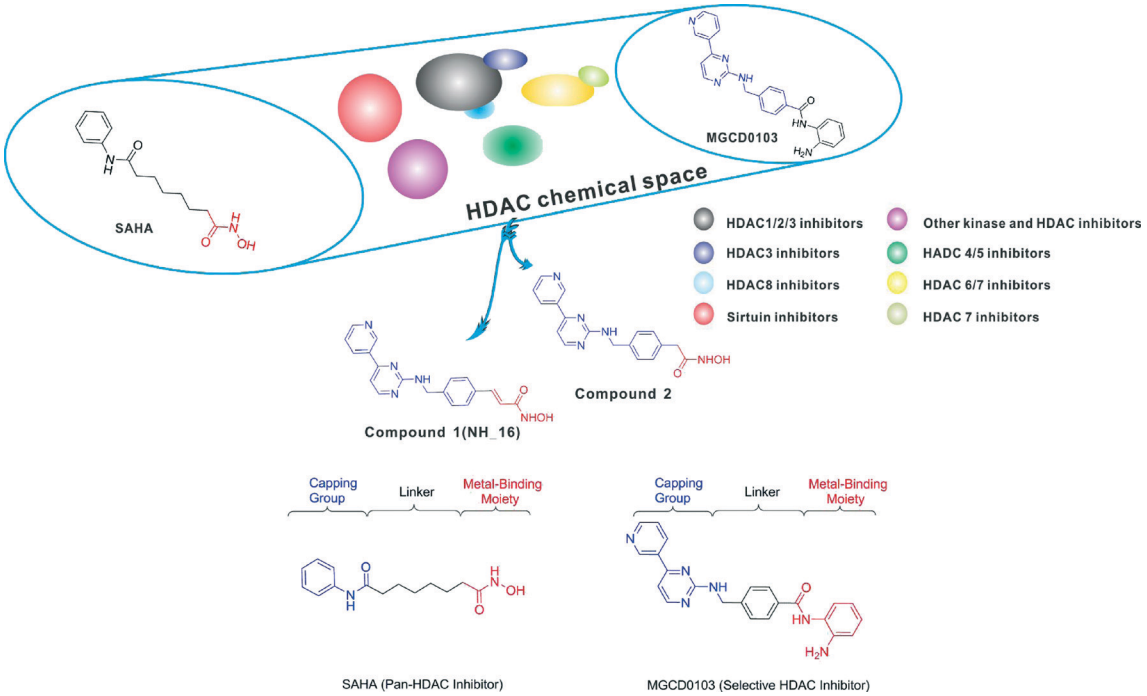

Fig. 1 Targeted compounds **1** and **2** obtained by visual screening. These two compounds were assembled by employing the ZBG moiety of SAHA and the Cap and linker fragment of MGCD0103. The classification of the HDAC chemical space from SAHA to MGCD0103 was subjectively based on the analysis of a recently published paper on HDAC inhibitors.

Almost all the clinical HDAC candidates can contain these above three basic moieties, and each part of the molecules seems to be the most optimal fragment as to itself.

Currently, a lot of *para*-substituted benzohydroxamic acids[9–12] and *para*-substituted cinnamic hydroxamic acids[13–17] are reported as multipotent HDAC inhibitors, and a certain number of them are being evaluated in clinical trials as anticancer preparations. Based on the information above, it has been hypothesized that novel HDIs can be developed through modifying the ZBG region among these important clinical HDAC inhibitors. We also observed the differences between MGCD0103 and SAHA in terms of their pharmacological properties and selectivity for isoforms of HDAC proteins. For example, SAHA has a relatively short half-life in plasma ($t_{1/2}$ = 2 h (ref. 18)) than MGCD0103 ($t_{1/2}$ = 9 h (ref. 19)). SAHA can inhibit the activity of all 11 known human class I and class II HDACs,[20] while MGCD0103 has strong isotype selectivity to HDAC1 and some weak inhibition against HDAC2, -3, and -11.[21] In addition, MGCD0103 could produce multiple responses in both lymphoma and AML clinical trials compared to SAHA.[22] Therefore, as shown in Fig. 1, we have designed and synthesized two new HDAC inhibitors, compounds **1** and **2** (Scheme 1), by recombining the selective HDAC inhibitor MGCD0103 and pan-HDAC inhibitor SAHA (the detailed procedure is available in the design section below, and chemistry details are given in the ESI),† which were expected to combine the longer half-life potency of MGCD0103 and the extensive inhibition against HDACs of SAHA. Their exclusive biological activities were preliminarily illustrated by the *in vitro* antiproliferative assay, apoptosis and cell cycle assay, *in vitro* HDAC inhibition fluorescence assay, *in vitro* stability assay and immunofluorescence microscopy detection.

Results and discussion

In vitro antiproliferative assay

We used 5 common tumor cell lines to investigate the antiproliferative effect of the two compounds (compound **1** and compound **2**) compared with their templates (MGCD0103 and SAHA) using the MTT method. The results revealed that compounds **1** and **2** displayed an anti-proliferative effect in a time-dependent and dose-dependent manner (Table 1 and Fig. S5 in the ESI†). The two compounds exhibited better effects than SAHA in A549, Hela, HepG2 and MCF7 cell lines, suggesting that they regenerate longer half-life potency by combining the MGCD0103 capping group and the SAHA metal-binding moiety. Further research will be focused on the stability and comparison of the two compounds and their templates (MGCD0103 and SAHA) *in vitro* and *in vivo*. Apoptosis and cell cycle arrest could both contribute to the antiproliferative effect. Thus, it is necessary to investigate the effect of the two compounds on apoptosis and cell cycle in the following section.

Apoptosis and cell cycle assay

HDIs could elicit a number of biological effects on cancer cells, such as apoptosis and cell-cycle arrest. Interestingly, compounds **1** and **2** induced apoptosis in Hela cells in a dose-dependent manner as well as MGCD0103 and SAHA. At

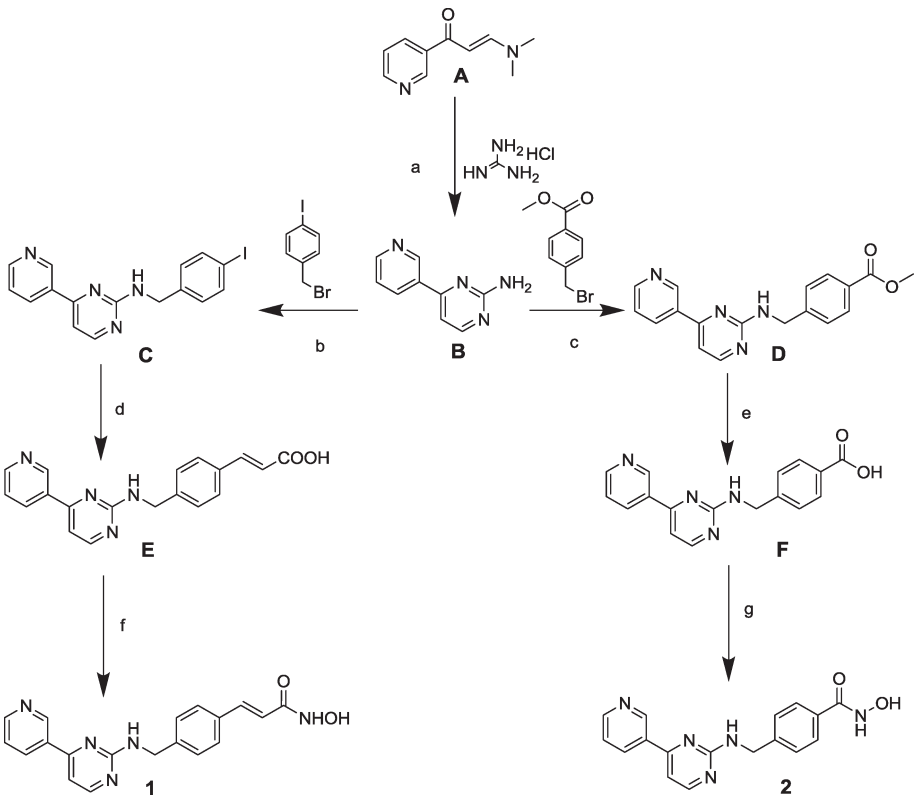

Scheme 1 The synthesis routes of compounds **1** and **2**.

a higher concentration of 5 μM, these two compounds exhibited a better pro-apoptotic effect than SAHA, although there was a little difference between MGCD0103 and the two compounds (Fig. 2). Cell cycle profiles of Hela treated with compounds **1** and **2** by flow cytometry demonstrated that both of them can induce the G1 phase arrest in which there is a significant G1-phase increase and an S-phase decrease with an increase in drug concentration. In addition, it was notable that both compounds could also give rise to an obvious G2-phase decrease at a high concentration (2 μM, Fig. 3).

Table 1 Antiproliferative activities of the designed compounds against five common cancer cells

Cancer cells	Compounds	Inhibition IC_{50} (μM)		
		24[a]	48[a]	72[a]
A549	MGCD0103	59.90	14.57	11.87
	SAHA	78.76	5.37	12.46
	1	97.96	8.32	7.99
	2	nd[b]	11.90	4.64
Hela	MGCD0103	43.80	3.32	3.42
	SAHA	7.13	9.19	8.96
	1	53.44	3.79	3.24
	2	30.67	7.23	3.17
HepG2	MGCD0103	5.79	4.05	4.25
	SAHA	10.77	10.52	8.78
	1	20.46	5.95	6.52
	2	22.92	4.03	2.96
HCT116	MGCD0103	29.69	1.24	3.51
	SAHA	32.46	5.06	<1.18
	1	8.28	<0.81	1.05
	2	13.70	<0.88	1.66
MCF-7	MGCD0103	84.17	56.81	2.49
	SAHA	54.55	28.66	9.59
	1	46.03	23.04	2.66
	2	45.98	16.03	2.41

[a] Time incubated with drugs. [b] ND = not determined.

In vitro HDAC inhibition fluorescence assay

The selectivity issue between MGCD0103 and SAHA commonly lies in the inhibition of the HDAC6 protein, and Stuart L. Schreiber identified that the *o*-aminoanilide element within HDIs could render such inhibitors inactive toward HDAC6 in cells.[23] Nevertheless, the individual modification of the capping group and the linker could also disturb the selectivity of HDIs, and more importantly, we cannot ignore that the combination of modifications at these three different regions is likely important for selective inhibitors.[3] Therefore, discussion as to the selectivity of compounds **1** and **2** for the HDAC6 protein should be more attractive.

In order to explore the *in vitro* HDAC inhibition, all compounds mentioned above (SAHA, MGCD0103, compound **1** and compound **2**) were subjected to enzyme inhibitory assays against HDAC1, HDAC2, HDAC3, and HDAC6. The results presented in Table 2 reveal that two new compounds (compound **1** and compound **2**) exhibited more potent activity against HDAC1, HDAC2, and HDAC3 than the standards (SAHA and MGCD0103). In terms of HDAC6, MGCD0103 with an *o*-aminoanilide moiety has no activity, while the other

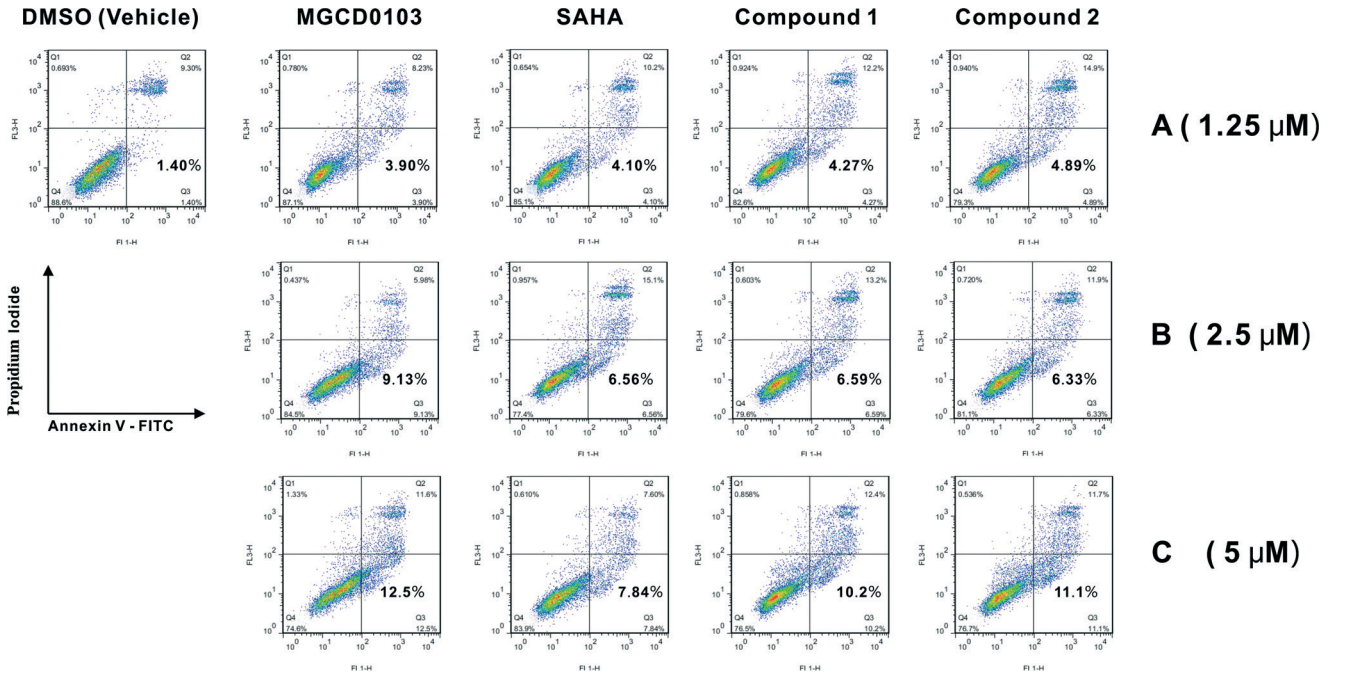

Fig. 2 Apoptosis assay on human cancer Hela cells by flow cytometry. Four compounds (MGCD01013, SAHA, and compounds **1** and **2**) were used at three different doses (A: 1.25 μM, B: 2.5 μM, C: 5 μM).

three compounds (SAHA, compound **1**, and compound **2**) with a hydroxamic acid moiety perform well.

Immunofluorescence microscopy

The HDAC inhibition assay has also been performed using the A549 cell line by immunofluorescence microscopy, and the results show consistency with the *in vitro* assay. In accord with SAHA, compounds **1** and **2** with hydroxamic acid in the ZBG region markedly increased the expression levels of both acetylated tubulin and acetylated histone, implying that the capping group and the linker from MGCD0103 cannot contribute to the change in HDAC6 selectivity and the *o*-aminoanilide moiety is a key factor in the selective HDIs (Fig. 4).

In vitro stability assay

In vitro stability assay was also conducted to compare the two compounds and their templates (SAHA and MGCD0103) in terms of stability. P. G Wang had reported that *in vitro* data can provide strong evidence to *in vivo* properties.[24] So based on our *in vitro* data (Table 3), compounds with the MGCD0103 capping group (compound **1**, compound **2** and MGCD0103) were superior to SAHA in half-life potency.

Conclusions

In summary, we focused on and investigated the known clinical HDAC inhibitors and obtained two potential HDAC inhibitors by fragment-based drug design (FBDD). The two compounds (compound **1** and compound **2**) directly from the optimized scaffolds of known clinical HDAC candidates SAHA and MGCD0103 combined both the advantages of SAHA and MGCD0103. Based on the results of the experiments above, they inherited the longer half-life potency derived from MGCD0103 and the non-selectivity toward HDAC6 derived from SAHA. To the best of our knowledge, both compounds (compound **1** and compound **2**) could be considered as novel histone deacetylase inhibitors in targeted drug development and possibly anticipated to be more effective under the clinical trials.

Design section

Sixteen known HDAC candidates in the clinical trials plus compound **24** (ref. 25) were selected for the design of novel HDAC inhibitors (Fig. 5). Focusing on modifications at the Zn-binding region of these canonical HDAC inhibitors, we step by step replaced this kind of group with three different moieties (hydroxamic acid, *o*-aminoanilide, and the newly reported 3-hydroxypyridin-2-thione (ref. 26)) and finally obtained thirty-four novel HDAC inhibitors.

Molecular docking was widely acceptable for virtual screening in the fragment-based drug design (FBDD). In this manuscript, we chose three kinds of available HDAC protein crystal complexes (HDAC2, PDB code: 3MAX; HDAC4, PDB code: 2VQW; HDAC8, PDB code: 1W22) as the docking receptors. Subsequently, the thirty-four designed HDAC inhibitors (Fig. 5) were docking into the Zn^{2+} ion active pocket of the three HDAC proteins, respectively. All the docking studies were performed using the Discovery Studio 3.5 suite. The Consensus Score based on the CDOCKER_INTERACTION_ENERGY of these three HDAC proteins with designed molecules was the final criterion (Table 4). The results showed that compounds NH_6, 9, 13 and 16 were ranked in the top of the docking

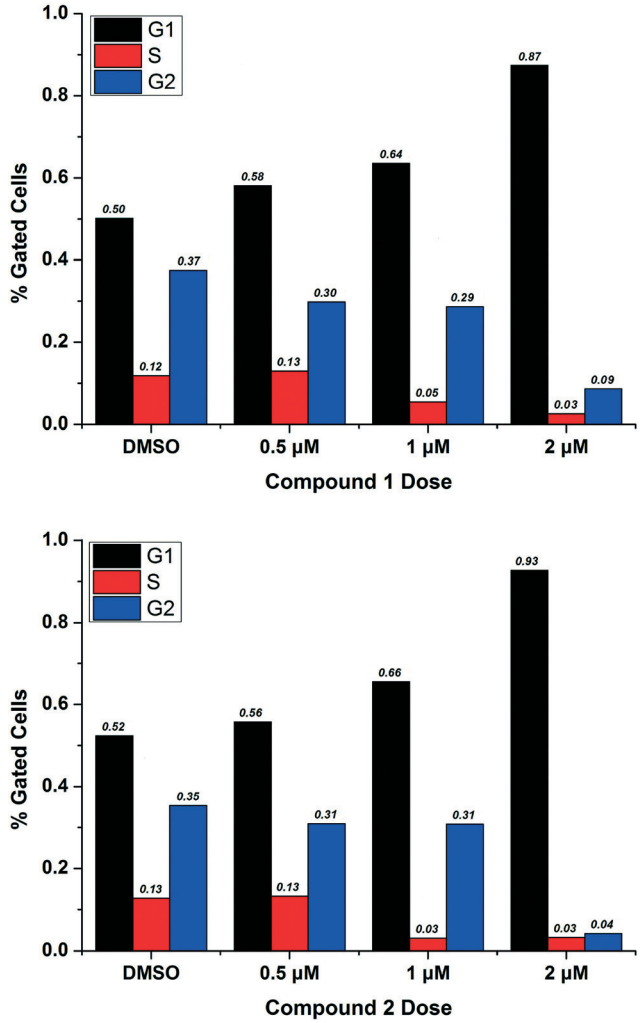

Fig. 3 Cell cycle profiles of compounds **1** and **2** on Hela cells at three different doses (0.5, 1, and 2 μM, respectively).

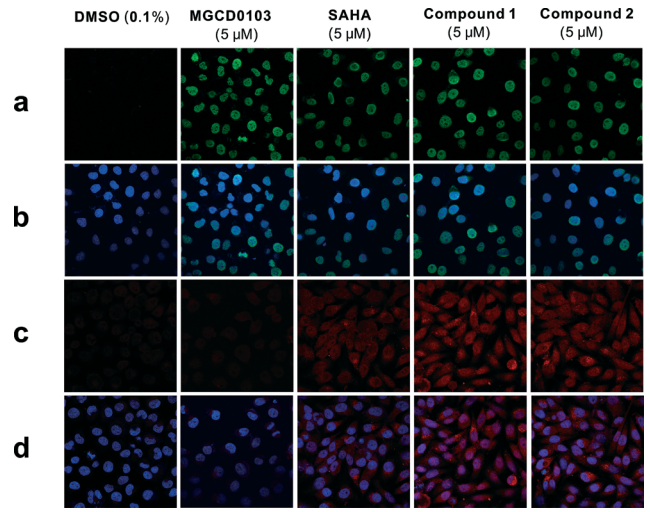

Fig. 4 Immunofluorescence microscopy detection in A549 cells of acetylated histones (row a); acetylated histones and DAPI nuclear staining (row b); acetylated tubulin (row c); acetylated tubulin and DAPI nuclear staining (row d). Cells were treated for 12 h with the indicated compounds (columns).

energy. Considering the difficulty of the syntheses of these four compounds and the reliability of the molecule design, we selected NH_16 (compound **1**) as the starting point. Meanwhile, we omitted the double bond and shortened the chain length in the structure of compound **1** to obtain compound **2**. As shown in Fig. 1, both compounds are the fusion of the MGCD0103 capping group and the SAHA metal-binding moiety. MGCD0103 has a longer half-life in plasma ($t_{1/2}$ = 9 h (ref. 19)) than SAHA ($t_{1/2}$ = 2 h (ref. 18)), while the SAHA metal-binding moiety which is hydroxamic acid has been reported to be interrelated to HDAC6 selectivity.[23] Hopefully, the designed compounds **1** and **2** can combine the advantages of MGCD0103 and SAHA just like combining their fragments (Table 5).

Table 2 *In vitro* inhibition of HDAC isoforms of SAHA, MGCD0103, compound **1** and compound **2**[a]

	IC_{50} of HDACs (μM)			
Compounds	HDAC1	HDAC2	HDAC3	HDAC6
SAHA	0.091	0.193	0.126	0.098
1	0.082	0.187	0.113	0.069
2	0.065	0.134	0.102	0.078
MGCD0103	0.171	0.283	1.165	>10

[a] Assays were performed several times ($n \geq 2$); the SD values are <20% of the mean.

To further validate the roles of the *o*-aminoanilide moiety of MGCD0103 and the hydroxamic acid moiety of SAHA in the HDAC6 selectivity, we generated the two HDAC6 homology models by comparative protein modeling (modeler) on the ModWeb server,[27] in which Model 1 was built based on the HDAC4 protein crystal complex (PDB code: 4CBT) and the sequence identity was 52%, while Model 2 was built based on the a HDAC7 protein crystal complex (PDB code: 3C10) and the sequence identity was 51% (Fig. 6a). The docking studies of these four compounds on these two protein models were subsequently performed using the CDOCKER algorithm developed on the CHARMM force field.[28] It is noteworthy that the chelating interaction of compounds with the Zn^{2+} ion can play a key role for the binding mode. As observed with the original ligands (9F4 in the 4CBT protein and Trichostatin A in the 3C10 protein), the two oxygen atoms at the hydroxamic acid moiety of compounds **1**, **2**, and SAHA could be much closer to the Zn^{2+} ion, and the distance between the O atom and the Zn^{2+} ion ranged from 2 to 4 Å (Fig. 6b). As to the *o*-aminoanilide fragment of MGCD0103, although some model[12] showed that the carbonyl-oxygen and the ortho-NH2 groups could directly interact with the Zn^{2+} ion and the distance between the carbonyl-oxygen and Zn^{2+} ion in the Model 1 protein was much closer, just 2.2 Å, this kind of moiety actually could not be accommodated well in the HDAC6 deep pocket. For example, the binding mode in the Model 2 protein seemed very impractical, in which the distance between the carbonyl-oxygen and the Zn^{2+} ion was 6.1 Å (Fig. 6b). Moreover, the

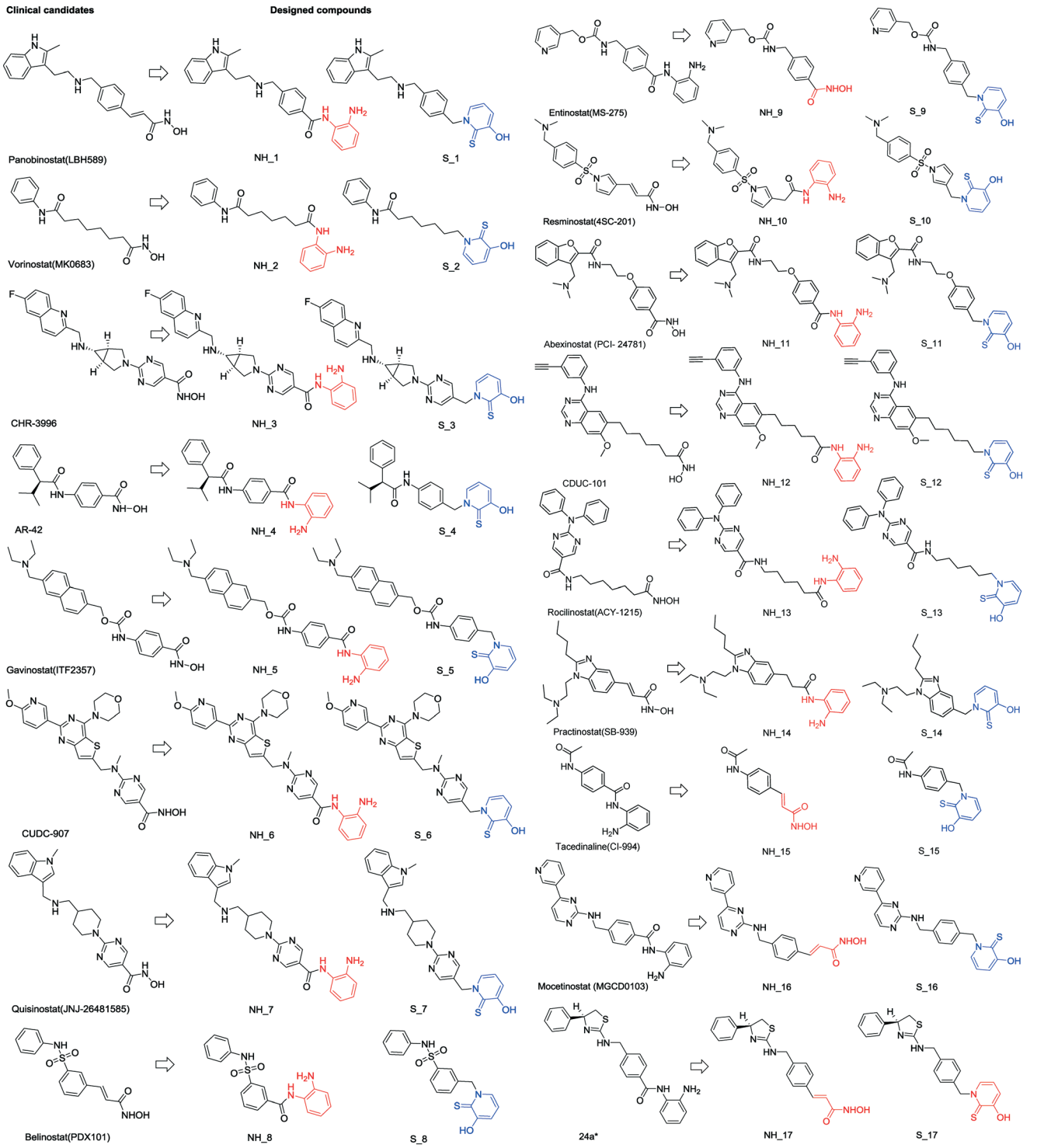

* referred to that this compound was abstracted from ref 1.

Fig. 5 Designed small molecule HDAC inhibitors based on clinical candidates except compound **24a**. *Refers to the compound abstracted from ref. 1.

docking energies of these four compounds were ranked and indicated that SAHA and compounds **1** and **2** can prefer the HDAC6 protein.

In summary, we cut the clinical drugs into fragments and generated new compounds by structural manipulations, including linking, merging and growth. With the process of molecular docking, two compounds (compound **1** and compound **2**) stood out. Then, HDAC6 homology models are generated to validate their HDAC6 selectivity. While SAR of clinical drugs as well as its fragments has been discussed before, our design leads to further optimization of selectivity and half-life potency. These two designed compounds are expected to have longer half-life potency like MGCD0103 and extensive inhibition against HDACs like SAHA.

Table 3 *In vitro* stability of SAHA, compound **1**, compound **2** and MGCD0103

	Stability ($t_{1/2}$)			
In vitro conditions	SAHA	Compound **1**	Compound **2**	MGCD0103
Artificial gastric fluid	22 h	>24 h	>24 h	>24 h
Artificial intestinal fluid	>24 h	>24 h	>24 h	>24 h
Plasma (mouse)	3 h	10 h	12 h	10 h
Microsome (mouse)	80 min	150 min	172 min	157 min

Chemistry section

The syntheses of compound **1** and compound **2** are described in Scheme 1. The synthesis of compound **B** started by mixing 3-(dimethylamino)-1-(pyridin-3-yl) prop-2-en-1-one (compound **A**) and guanidine hydrochloride in Bu-OH, and then the solution was heated to reflux overnight. With the reaction of nucleophilic substitution, compound **C** and compound **D** were obtained, respectively, from compound **B**. Compound **C** was further subjected to Heck reaction and gave compound **E**. Compound **F** was simply obtained by the hydrolysis reaction from compound **D**. Under the same conditions, compound **E** and compound **F** were converted to the target hydroxamic acid compound **1** and compound **2**, respectively.

Conditions: a) NaOH, *n*-BuOH, reflux, overnight; b, c) NaH, THF, rt, 8 h; d) CH_2═CHCOOH, $Pd_2(bda)_3$, POT, Et_3N, DMF, 100 °C, overnight; e) MeOH, H_2O, NaOH, HCl, rt, 2 h; f, g) NH_2OTHP, EDC, HOBt, DMF, 50 °C, 6 h.

Table 4 Results of virtual screening by molecular docking based on three human HDAC protein crystal structures (HDAC2, PDB code: 3MAX; HDAC4, PDB code: 2VQW; HDAC8, PDB code: 1W22)

Designed compounds	CDOCKER_INTERACTION_ENERGY (kcal mol^{-1})[a]			Consensus score[b]
	3MAX	2VQW	1W22	
NH_6	−44.8109	nd[c]	−42.5724	2
NH_9	−43.7696	−63.3461	−52.8084	2
NH_13	−55.5114	nd	−45.9295	2
NH_16	−40.0754	−57.4949	−47.1285	2
S_6	−44.7454	nd	−48.3771	2
S_13	−44.9942	−63.5364	−38.4227	2
NH_4	−31.5481	−57.4348	−35.4223	1
NH_10	−44.9379	−56.2177	−35.7044	1
NH_11	−45.1783	−11.9014	−38.7428	1
NH_12	−53.3811	nd	−40.5981	1
NH_17	−40.5589	−43.6633	−46.5146	1
S_1	−36.9707	−58.1268	−30.5661	1
S_9	−44.7117	−56.9281	−43.222	1
S_16	−33.3572	−57.5656	−33.4615	1
NH_1	−33.4412	−52.4794	−34.4908	0
NH_2	−34.5862	nd	−37.0525	0
NH_3	−37.8038	−53.6372	−37.1858	0
NH_5	−35.2228	−54.1914	−38.3205	0
NH_7	−41.5533	−22.9162	−37.4001	0
NH_8	−33.7839	−53.1635	−35.1557	0
NH_14	−43.8521	nd	−36.3722	0
NH_15	−30.7174	−52.1275	−41.3081	0
S_2	−32.5077	−56.2285	−30.3053	0
S_3	−37.6851	−43.3897	−35.9425	0
S_4	−30.8318	−27.3182	−33.1053	0
S_5	−38.9497	nd	−36.1872	0
S_7	−42.9461	−56.2321	−32.92	0
S_8	−26.8635	−50.047	−28.6409	0
S_10	−31.983	−49.8078	−34.0877	0
S_11	−41.6823	nd	−31.5389	0
S_12	−38.6814	−2.01496	−37.4977	0
S_14	−37.6577	−1.67183	−34.8718	0
S_15	−33.41	−47.7369	−39.4122	0
S_17	−29.3918	−46.6355	−33.2257	0

[a] Molecular docking assays were performed using the Discovery Studio 3.5 software suite, in which the CDOCKER algorithm is the main docking protocol. [b] The Consensus Score protocol in Discovery Studio uses the entire set of poses across all molecules to rank order your output; simply saying, if the value of docking energy for each target protein is ranked into the top 20% of the entire molecules, the value of the Consensus score will be added one. [c] nd: no data.

Biological section

Antiproliferative assay by the MTT method. All cell lines (A549, Hela, HepG2, HCT116, and MCF-7) were maintained in DMEM or RPMI-1640 medium containing 10% fetal bovine serum at 37 °C, in a 5% CO_2 humidified incubator. Cell proliferation assay was determined by the MTT method. Briefly, cell lines were passaged the day before seeding into 96-well plates, allowed to grow for 12 h, and then treated with different concentrations of compounds for 24 h, 48 h, and 72 h, respectively. A 5 mg ml^{-1} MTT solution was added to each well. After incubation for another 4 h, the medium inside was carefully removed and 100 μL of DMSO was added. After shaking for 15 min, the absorbance was determined using an ELISA reader at 570 nm. Each experiment was performed triplicate, and dose-dependent curves were calculated using Origin 8.6. The detailed results are shown in Fig. S5.†

Induced apoptosis by flow cytometry. To detect apoptosis induced by compounds **1** and **2**, Hela cells were seeded per well in 24-well plates and were incubated overnight. Then,

Table 5 The docking energies of MGCD0103, SAHA, and compounds **1** and **2** on the homology modeling of HDAC6

Compounds	CDOCKER_ENERGY (kcal mol^{-1})[a]	
	Model 1 protein	Model 2 protein
SAHA	−38.45	−46.34
1	−32.75	−36.01
2	−32.55	−30.87
MGCD0103	−25.69	−24.12

[a] Molecular docking assays were performed using the Discovery Studio 3.5 software suite, in which the CDOCKER algorithm is the main docking protocol.

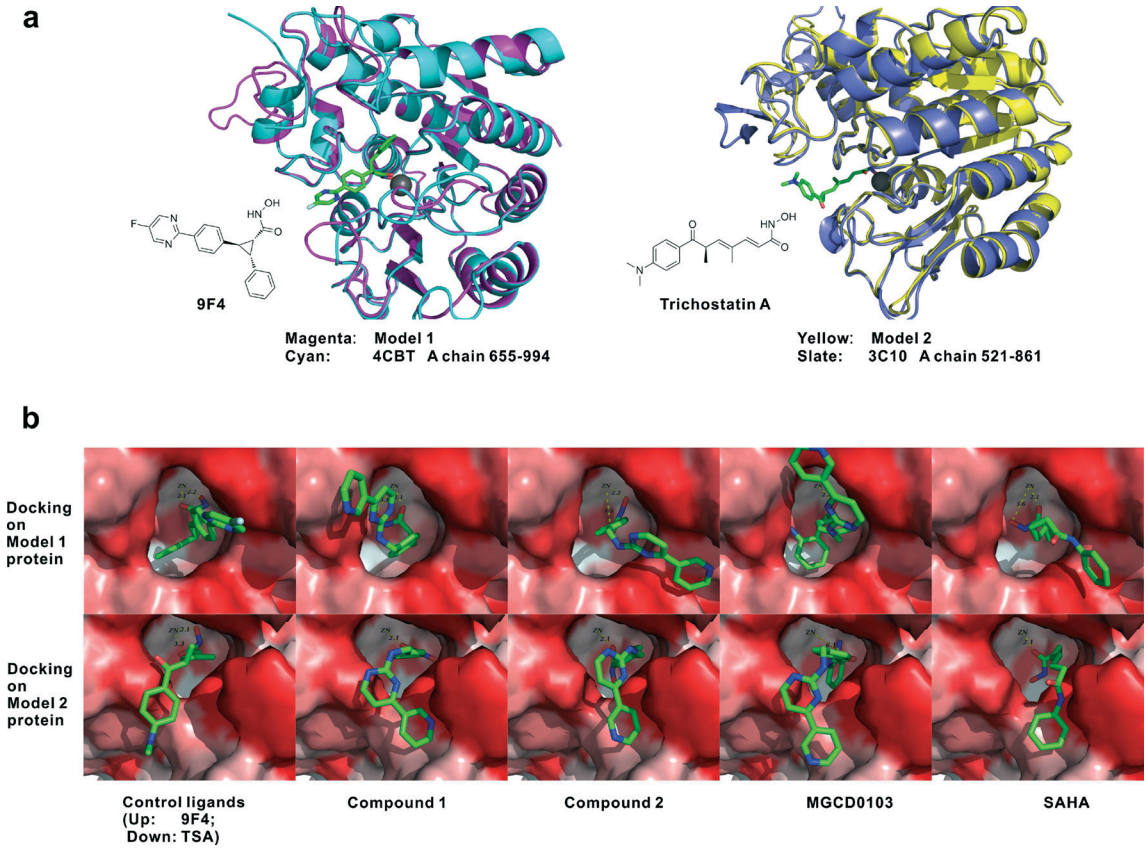

Fig. 6 The results of homology modeling and molecular docking on the HDAC6 protein. (a) Two homology models of HDAC6 by the ModWeb server in the Sali Lab (Modeller): one template is the continuous segment of residues between 655 and 994 of the A chain of 4CBT, an HDAC4 protein crystal complex with a small molecule 9F4 in the protein data bank (PDB); the other one is the continuous segment of residues between 521 and 861 of the A chain of 3C10, an HDAC7 protein crystal complex with a small molecule Trichostatin A (TSA) in the protein data bank (PDB); (b) docking modes of compounds **1**, **2**, MGCD0103, and SAHA based on Model 1 and Model 2; all the figures were drawn using Pymol 1.6, and the red regions represented the hydrophobic surface.

cells were treated with compounds **1** and **2** at three different concentrations (1.25 μM, 2.5 μM and 5 μM, separately). MGCD0103 and SAHA were chosen as positive controls, and DMSO was chosen as the negative control. After 48 h, cells were harvested for apoptosis detection. In brief, collected cells were washed once with PBS and subsequently washed once with binding buffer and then stained with FITC conjugated Annexin V and propidium iodide (PI) in the binding buffer for 20 min at room temperature in the dark. Apoptotic cells were quantified using a FACScan cytofluorometer (PT. Madagasi Brosa Inc., JI. Batang Hari No. 73, Propinsi Sumatera Utara, Indonesia) plotting at least 10 000 events per sample. To quantify the data, the frequencies in all quadrants were analyzed using the FlowJo software. We regarded cells in the lower right quadrant (Annexin V positive/PI negative) as early apoptotic cells, and cells in the upper right quadrant (Annexin V positive/PI positive) as late apoptotic cells and necrotic cells.

Cell cycle assay by flow cytometry. To detect the effect of compounds **1** and **2** on cell cycle, Hela cells were treated with compounds **1** and **2** at the gradient concentrations (0.5 μM, 1 μM and 2 μM), and DMSO was used as the negative control. After 24 h, cells were harvested, washed with PBS once, and fixed in PBS containing 75% ethanol at −20 °C overnight. Then, cells were collected by centrifugation and subsequently resuspended in PBS containing 0.1 mg mL^{-1} RNase A and 5 μg mL^{-1} propidium iodide (PI) and kept in the dark for 30 min before the cell cycle detection. Cellular DNA content, for cell cycle distribution analysis, was measured by flow cytometry using a FACScan cytofluorometer plotting at least 10 000 events per sample. The percentage of cells in the G0/G1, S and G2/M phases of the cell cycle was determined using the modfit software.

***In vitro* HDAC inhibition fluorescence assay.** Firstly, 10 μL of enzyme solution (Hela nuclear extract, HDAC1, HDAC2, HDAC3 or HDAC6) and various concentrations of the four compounds (SAHA, MGCD0103, compound **1** and compound **2**) were mixed. The mixture was incubated at 37 °C for 5 min, and then fluorogenic substrate Boc-Lys(acetyl)-AMC (40 μL) was added. After incubation of 37 °C for 30 min, the mixture was stopped by adding 100 μL of developer containing trypsin and TSA. 20 min later, fluorescence intensity was measured using a microplate reader at excitation and emission wavelengths of 390 and 460 nm, respectively. The inhibition

ratios were calculated from the fluorescence intensity readings of tested wells relative to those of control wells, and the IC_{50} values were calculated using a regression analysis of the concentration/inhibition data.

Immunofluorescence microscopy procedures. A549 cells were seeded on cover slips and incubated at 37 °C. After 24 h, the medium was replaced with a medium containing 0.1% DMSO, or diluted with test compounds (5 μM SAHA, 5 μM MGCD0103, 5 μM compound **1**, 5 μM compound **2**) containing 0.1% DMSO, and incubated at 37 °C. After 24 h, the cells were fixed (see below for fixation protocols) and incubated with antibodies and stains (see below for antibody detection and staining protocols). All the images were captured using a Nikon confocal microscope (C2+, Nikon, Tokyo, Japan) and analyzed using the Nis-element advanced research software (Nikon).

Fixation protocols

Tubulin. The medium was aspirated, and the cover slips were incubated with 400 μL of fixation solutions (4% glutaraldehyde solution of PBS) for 20 min. The fixation solution was then aspirated, and the cover slip was rinsed with PBS/0.1% Triton-X-100 for 3 × 5 min. The cover slip was then incubated with 300 μL of a 10 mg mL^{-1} sodium borohydride solution in PBS for 10 min. This solution was aspirated, and the cover slip was rinsed with 400 μL of PBS for 3 × 5 min. The cover slip was then blocked with 2% bovine serum albumin for 10 min.

Histone. The medium was aspirated and replaced with 300 μL of 5% acetic acid/ethanol (−20 °C), and this was incubated for 3 min. The acetic acid/ethanol solution was then aspirated, and the cover slip was rinsed with PBS. The cover slip was then incubated with 300 μL of PBS/0.5% Triton-X-100 for 10 min. This solution was then aspirated, and the cover slip was blocked with 2% bovine serum albumin for 10 min.

Antibody detection/staining protocol. Cover slips fixed for optimal tubulin visualization were incubated with anti-acetylated tubulin antibody (Sigma monoclonal clone 6-11B-1) in BSA (1 : 300 dilution) for 1 h at 37 °C. Cover slips fixed for optimal histone visualization were incubated with anti-acetylated lysine antibody (Cell Signaling monoclonal Ac-K-103) in BSA (1 : 200 dilution) for 1 h at 37 °C. Cover slips were then washed 3 × 5 min with 300 μL of PBS/0.1% Triton-X-100. Cover slips were then incubated with secondary antibody (1 : 400 Molecular Probes Alexa Fluor® 594 goat anti-mouse IgG in BSA for tubulin and 1 : 200 Molecular Probes Alexa Fluor® 488 goat anti-mouse IgG in BSA for histone) for 1 h at 37 °C in the dark. After subsequent washing (3 × 5 with 400 μL of PBS/0.1% Triton-X-100), all cover slips were stained with DAPI staining solution (Beyotime 10 mg mL^{-1} stocked diluted 1 : 1000 in BSA) for 20 min in the dark. All cover slips were then washed extensively in the dark (3 × 5 min with 300 μL of PBS, 1 × 5 min with 300 μL of ddH_2O) prior to mounting.

Homology and molecular modeling

Homology modeling. Human HDAC6 sequences were obtained from the NCBI database (http://www.ncbi.nlm.nih.gov/protein/AAH69243.1). Because the HDAC6 has two catalytic subunits, we chose the second one (CDII, Gly482-Gly800) as the major functional domain in the HDAC6 protein. In the next step, we submitted this sequence into the ModWeb server maintained by the Sali group (https://modbase.compbio.ucsf.edu/modweb/). Note that we chose the "Slow (Seq-Prf, PSI-Blast)" as the fold assignment method that made our model more accurate. Two models (Models 1 and 2) have been obtained, in which Model 1 was built on the HDAC4 protein crystal complex (PDB code: 4CBT) as the template, and the sequence identity was 52%, while Model 2 was built on the HDAC7 protein crystal complex (PDB code: 3C10) as the template, and the sequence identity was 51%.

To adjust the position of zinc at the catalytic site, Model 1 was superimposed over the crystal structure of 4CBT by the protein structure similarity method of the Discovery Studio 3.5 suite, while Model 2 was superimposed over the crystal structure of 3C10 in the same way. Finally, an energy minimization was performed, and the homology modeling procedure was completed.

Molecular docking. Molecular docking of compounds into the three-dimensional protein structure of human HDAC6 (Models 1 and 2) was carried out using the Discovery Studio (version 3.5) as implemented through the graphical user interface DS-CDOCKER protocol. The three-dimensional structures of the aforementioned compounds were constructed using the Chem. 3D ultra 12.0 software [Chemical Structure Drawing Standard; Cambridge Soft Corporation, USA (2010)], and then, they were energetically minimized by using MMFF94 with 5000 iterations and minimum RMS gradient of 0.10. All bound waters and ligands were eliminated from the protein, and polar hydrogen was added to the proteins. Each compound would retain 20 poses and was ranked by CDOCKER ENERGY. The selection of the conformation of each compound would partly depend on the binding mode in the active pocket, when compared to those known control such as 9F4 and TSA.

Abbreviations

FBDD	Fragment-based drug design
HDIs	Histone deacetylase inhibitors
HDAC	Histone deacetylase
HAT	Histone acetyltransferase
ZBG	Zn-binding group
TSA	Trichostatin A

Acknowledgements

This work was supported by the Natural Science Foundation of Jiangsu Province (No. BK20130554), by Major Projects Control and Rectification of Water Body Pollution (2011ZX07204-001-004), and by National Science & Technology Pillar Program during the Twelfth Five-year Plan Period (No. 2012BAD36B01).

References

1 O. Khan and N. B. La Thangue, HDAC inhibitors in cancer biology: emerging mechanisms and clinical applications, *Immunol. Cell Biol.*, 2012, **90**, 85–94.
2 A. L. Clayton, *et al.*, Enhanced histone acetylation and transcription: a dynamic perspective, *Mol. Cell*, 2006, **23**, 289–296.
3 A. V. Bieliauskas and M. K. Pflum, Isoform-selective histone deacetylase inhibitors, *Chem. Soc. Rev.*, 2008, **37**, 1402–1413.
4 R. Benedetti, *et al.*, Targeting Histone Deacetylases in Diseases: Where Are We?, *Antioxid. Redox Signaling*, 2015, **23**, 99–126.
5 P. A. Marks and R. Breslow, Dimethyl sulfoxide to vorinostat: development of this histone deacetylase inhibitor as an anticancer drug, *Nat. Biotechnol.*, 2007, **25**, 84–90.
6 C. Campas-Moya, Romidepsin for the treatment of cutaneous T-cell lymphoma, *Drugs Today*, 2009, **45**, 787–795.
7 D. C. Rees, M. Congreve, C. W. Murray and R. Carr, Fragment-based lead discovery, *Nat. Rev. Drug Discovery*, 2004, **3**, 600–672.
8 P. J. Hajduk and J. Greer, A decade of fragment-based drug design: strategic advances and lessons learned, *Nat. Rev. Drug Discovery*, 2007, **6**, 211–219.
9 J. Hou, *et al.*, Discovery and extensive in vitro evaluations of NK-HDAC-1: a chiral histone deacetylase inhibitor as a promising lead, *J. Med. Chem.*, 2012, **55**, 3066–3075.
10 T. T. Tung, *et al.*, New benzothiazole/thiazole-containing hydroxamic acids as potent histone deacetylase inhibitors and antitumor agents, *Med. Chem.*, 2013, **9**, 1051–1057.
11 D. J. Witter, *et al.*, Benzo[b]thiophene-based histone deacetylase inhibitors, *Bioorg. Med. Chem. Lett.*, 2007, **17**, 4562–4567.
12 L. A. Hooven, *et al.*, Effects of suberoylanilide hydroxamic acid and trichostatin A on induction of cytochrome P450 enzymes and benzo[a]pyrene DNA adduct formation in human cells, *Bioorg. Med. Chem. Lett.*, 2005, **15**, 1283–1287.
13 C. T. Chan, *et al.*, Syntheses and discovery of a novel class of cinnamic hydroxamates as histone deacetylase inhibitors by multimodality molecular imaging in living subjects, *Cancer Res.*, 2014, **74**, 7475–7486.
14 C. Ning, *et al.*, Design, synthesis and biological evaluation of di-substituted cinnamic hydroxamic acids bearing urea/thiourea unit as potent histone deacetylase inhibitors, *Bioorg. Med. Chem. Lett.*, 2013, **23**, 6432–6435.
15 J. Hou, *et al.*, Structure-based optimization of click-based histone deacetylase inhibitors, *Eur. J. Med. Chem.*, 2011, **46**, 3190–3200.
16 L. Chen, *et al.*, Dual inhibitors of inosine monophosphate dehydrogenase and histone deacetylase based on a cinnamic hydroxamic acid core structure, *Bioorg. Med. Chem.*, 2010, **18**, 5950–5964.
17 S. Dallavalle, *et al.*, Design, synthesis, and evaluation of biphenyl-4-yl-acrylohydroxamic acid derivatives as histone deacetylase (HDAC) inhibitors, *Eur. J. Med. Chem.*, 2009, **44**, 1900–1912.
18 E. H. Rubin, *et al.*, A study to determine the effects of food and multiple dosing on the pharmacokinetics of vorinostat given orally to patients with advanced cancer, *Clin. Cancer Res.*, 2006, **12**, 7039–7045.
19 G. Garcia-Manero, *et al.*, Phase 1 study of the oral isotype specific histone deacetylase inhibitor MGCD0103 in leukemia, *Blood*, 2008, **112**, 981–989.
20 P. A. Marks, Discovery and development of SAHA as an anticancer agent, *Oncogene*, 2007, **26**, 1351–1356.
21 K. Ververis, *et al.*, Histone deacetylase inhibitors (HDACIs): multitargeted anticancer agents, *Biol.: Targets Ther.*, 2007, **7**, 47–60.
22 A. A. Lane and B. A. Chabner, Histone deacetylase inhibitors in cancer therapy, *J. Clin. Oncol.*, 2009, **27**, 5459–5468.
23 J. C. Wong, *et al.*, Structural biasing elements for in-cell histone deacetylase paralog selectivity, *J. Am. Chem. Soc.*, 2003, **125**, 5586–5587.
24 P. G. Wang, *et al.*, Discovery and extensive in vitro evaluations of NK-HDAC-1: a chiral histone deacetylase inhibitor as a promising lead, *J. Med. Chem.*, 2012, **55**, 3066–3075.
25 C. M. Marson, *et al.*, Discovery of potent, isoform-selective inhibitors of histone deacetylase containing chiral heterocyclic capping groups and a *N*-(2-aminophenyl)benzamide binding unit, *J. Med. Chem.*, 2013, **56**, 6156–6174.
26 V. Patil, *et al.*, 3-Hydroxypyridin-2-thione as novel zinc binding group for selective histone deacetylase inhibition, *J. Med. Chem.*, 2013, **56**, 3492–3506.
27 G. Wu, *et al.*, Detailed analysis of grid-based molecular docking: A case study of CDOCKER-A CHARMm-based MD docking algorithm, *J. Comput. Chem.*, 2003, **24**, 1549–1562.
28 U. Pieper, *et al.*, ModBase, a database of annotated comparative protein structure models, and associated resources, *Nucleic Acids Res.*, 2011, **39**, D465–D474.

